Dalton Transactions

ROYAL SOCIETY OF CHEMISTRY

COMMUNICATION

View Article Online
View Journal | View Issue

Check for updates

Cite this: *Dalton Trans.*, 2026, **55**, 107

Received 30th October 2025,
Accepted 1st December 2025

DOI: 10.1039/d5dt02617b

rsc.li/dalton

Open Access Article. Published on 19 December 2025. Downloaded on 6/17/2026 6:17:10 AM.
This article is licensed under a Creative Commons Attribution 3.0 Unported Licence.

Synthetic methods for key precursors of biologically active dimethylsulfoxide ruthenium complexes

Sreshtha Nayek, [a] Rodrigo S. Correa, *[a,b] Ehsan Ezzatpour Ghadim, *[a,d] Juliusz A. Wolny, [c] Volker Schünemann,[c] Rafael Cavalieri Marchi *[a,d] and Peter J. Sadler *[a]

Microwave- and sonication-assisted methods provide efficient synthesis of octahedral Ru(II) and Ru(III) S- and O-bound dimethyl sulfoxide (DMSO) complexes, precursors to anticancer, antimicrobial and anti-neurodegenerative drugs, in comparison with conventional hotplate (thermal) synthesis. In addition, sonication led to a novel O-bound DMSO oxo-bridged di-Ru(IV) complex, for which the X-ray structure, solvolysis, reduction by ferrocene, and Density Functional Theory (DFT) calculations are reported.

Ruthenium–DMSO complexes are widely used as precursors for the synthesis of various compounds of biological interest.[1–5] [ImH]*trans*-[$RuCl_4$(DMSO)(Im)] (DMSO = dimethyl sulfoxide, Im = imidazole) known as NAMI-A, was the first anticancer ruthenium drug to be screened in humans in 1999.[6] Its synthesis involves the precursor Ru(III) complex, [$(DMSO)_2H$] *trans*-[$RuCl_4(DMSO)_2$] (**1**, Fig. 1). Other Ru–DMSO complexes that are frequently used as precursors to anticancer drugs include *cis*-[$RuCl_2(DMSO)_4$] (**2**) and *trans*-[$RuCl_2(DMSO)_4$][7] (**3**), Fig. 1. These Ru(II) precursors have biological significance, including antibacterial activity against *Salmonella typhimurium* and *Escherichia coli*[8] and anticancer activity[9] enhanced with UVA irradiation.[10] They can bind to DNA bases, *e.g.* adenine and guanine,[11–13] and inhibit protein aggregation similar to NAMI-A to treat neurodegenerative diseases.[14,15]

Despite these applications, the synthesis of Ru–DMSO precursors **1–3** can present difficulties. The usual starting material $RuCl_3{\cdot}3H_2O$ has variability in water content, may contain Ru(IV) species besides Ru(III), and a poorly-defined Ru/Cl ratio.[1,16] Also, impurities in DMSO such as dimethylsulfide[17] and the sensitivity of the reaction to the duration and degree of heating, can contribute to a lack of reproducibility.

Commonly, **1–3** are obtained by hot-plate heating protocols. However, alternative synthetic methods based on microwave-assisted and ultrasound bath-assisted synthesis have already shown potential for use in synthesis of metal complexes[18–20] and inorganic materials in general.[21–24] With microwave treatment, rapid transfer of energy results in effective uniform heating of the reaction medium and reduced reaction times,[19,25] which can improve reproducibility by minimising thermal gradients and reducing variability between batches, allowing control of nucleation for metal–DMSO complexes.[26,27] In ultrasound treatment, the waves form local hotspots having extremely high-energy microenvironments[28] in a process called cavitation[29–31] that can promote the formation of high-oxidation-state species such as Ru(IV). Ni, Cd and Zn complexes containing indole Schiff bases with anticancer activity have been synthesised using this method.[32]

Both these methods offer strategies for accelerating synthesis and modulating electronic and/or structural outcomes that may otherwise be inaccessible *via* hotplate heating. Thus, they have been explored for M–DMSO precursors, where M = Pd, Pt, Rh, Ir, Os, and other metals,[2,33–35] precursors of interest in *e.g.* catalysis and energy conversion. The aim of the present work was to explore faster and more reproducible methods of synthesising biologically-relevant Ru–DMSO precursors using microwave and the less common sonication method.

Using hot-plate heating methods, precursors **1** and **2** (including polymorph **2′**) were obtained. In case of the microwave-assisted method, we investigated the effects of temperature, reaction times and HCl (37%) on the synthesis of Ru–DMSO precursors **2** and **3** aiming for higher reproducibility by varying these parameters, Table 1. The ultrasound bath-assisted reaction generated a novel redox-active diruthenium (IV) oxo-bridged compound, complex **4**, Fig. 1. The products were characterised by a combination of single crystal X-ray diffraction (SCXRD), powder X-ray diffraction (PXRD), UV-

[a]*Department of Chemistry, University of Warwick, Gibbet Hill Road, Coventry CV4 7AL, UK. E-mail: Ehsan.Ezzatpour-Ghadim.3@warwick.ac.uk, P.J.Sadler@warwick.ac.uk*
[b]*Department of Chemistry, Federal University of Ouro Preto, Ouro Preto 35402-136, Brazil. E-mail: rodrigocorrea@ufop.edu.br*
[c]*Department of Physics, RPTU University of Kaiserslautern-Landau, Erwin-Schrödinger-Str. 46, 67663 Kaiserslautern, Germany*
[d]*School of Engineering, University of Warwick, Gibbet Hill Road, Coventry CV4 7AL, UK. E-mail: Rafael.Cavalieri-Marchi@warwick.ac.uk*

Open Access Article. Published on 19 December 2025. Downloaded on 6/17/2026 6:17:10 AM.
This article is licensed under a Creative Commons Attribution 3.0 Unported Licence.

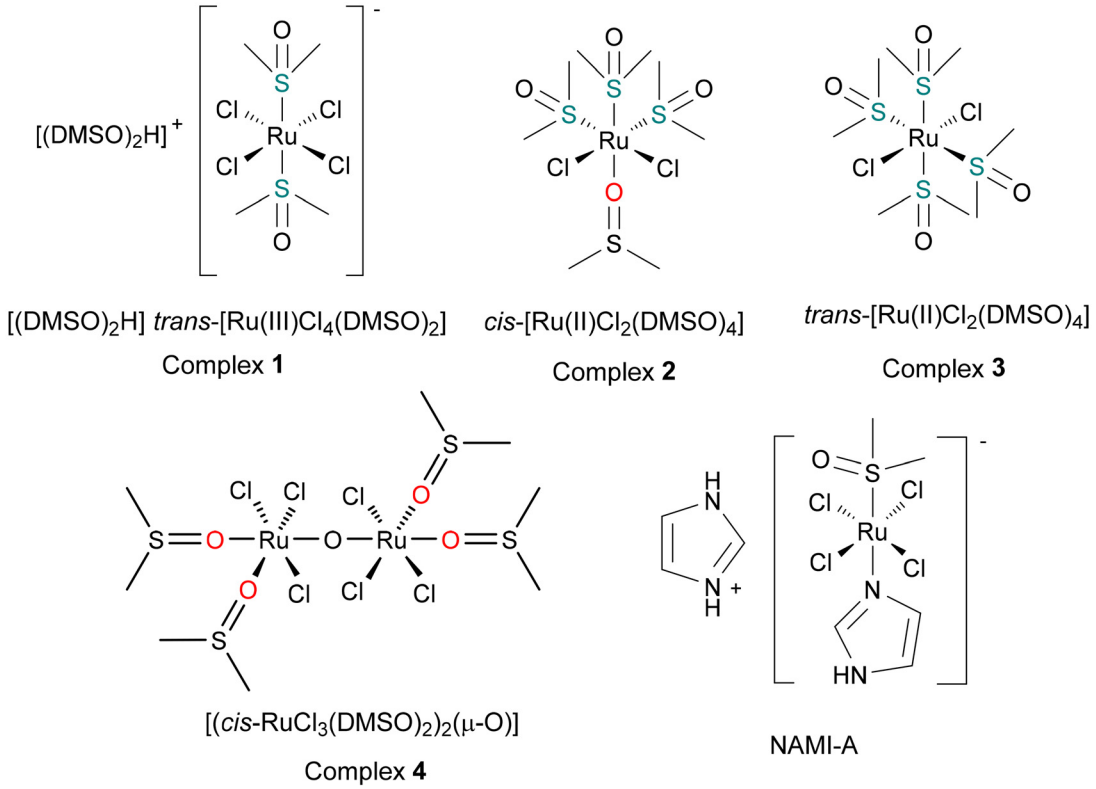

Fig. 1 Chemical structures of complexes **1–4** and NAMI-A.

visible spectroscopy, high-resolution mass spectrometry (HRMS), ^{1}H-NMR spectroscopy, elemental analysis and cyclic voltammetry (CV). In addition, the reduction of **4** by ferrocene was studied spectroscopically and with complementary Time-Dependent Density Functional Theory (TD-DFT) modelling.

Details of reaction protocols are described in Table 1, SI section S1.2, Scheme S1 and Table S1. The NMR, HRMS, CHN analysis, SCXRD and PXRD characterisations of **1–4** are described in the SI sections S1.3 and S1.4, Tables S2–S6 and Fig. S1–S4. The most reliable protocol to obtain **1** with high yield (65%) was **H1**. This method was used by Alessio *et al.*[36] and involves the dissolution of $RuCl_3{\cdot}3H_2O$ in hot ethanol, followed by reaction in DMSO + HCl.

Procedures **H2**, **H3** and majority of microwave protocols (**MW1–MW4**), under our conditions, gave **2** as product, confirmed by NMR, HRMS, SCXRD and PXRD data (SI section S1.4, Tables S2, S3 and S5, Fig. S1, S3 and S4). Reactions and characterisations were reproducible for at least 3 repeats for each condition. Additionally, hotplate protocol **H4** with the longest heating time yielded a polymorph of *cis*-$[RuCl_2(DMSO)_4]$, **2′**. Synthesis aided by microwave irradiation led to a considerable reduction in reaction time (to *ca.* 20 min) compared to hot-plate heating (>110 min) with comparable yields.

The reaction time influenced the yield of the microwave-assisted synthesis. Longer heating times at 373 K resulted in higher yields, increasing from 12% with 10 min heating (**MW1**) to 62% with 20 min heating (**MW3**). Moreover, when the microwave reaction was performed in the absence of HCl (**MW5**), complex **3** *trans*-$[RuCl_2(DMSO)_4]$ was formed as confirmed by NMR, HRMS, SCXRD and PXRD data, SI section S1.4, Tables S2, S3 and S5, Fig. S1, S3 and S4.

Normally, the presence of excess Cl^- in the reaction mixture leads predominantly to chlorido ruthenium products.[37] Here, the addition of Cl^- for **MW1–MW4** synthesis led to the formation of the *cis*-$[RuCl_2(DMSO)_4]$ isomer, while in its absence the *trans* isomer (**MW5**) was formed. This suggests that *cis*- and *trans*-directing effects may play a role in the reductive and/or ligand substitution processes during the reaction. Thus, the presence of HCl stabilises the formation of the more thermodynamically stable *cis* di-chlorido geometry.

The syntheses of **2** and **3** include a redox step in which Ru(III) is reduced to Ru(II). DMSO acts as a S- or O-bound ligand and also as a reducing agent, being oxidised to byproducts like the sulfone.[38] Substitution of the labile chloride and DMSO ligands by other ligands can be rate-limiting in the use of these precursors.[39–43]

Surprisingly, the sonication-assisted synthesis **S1** yielded an oxo-bridged diruthenium(IV) complex. Ultrasound waves can generate radicals either through water homolysis or by splitting atmospheric oxygen,[29–31] assisting the formation of an oxo bridge. The reaction was complete within 40 min with a 62% yield, and crystals of **4** were characterised by NMR, HRMS, SCXRD and PXRD (Table 1, Tables S2, S3 and S5 and

 This journal is © The Royal Society of Chemistry 2026

Open Access Article. Published on 19 December 2025. Downloaded on 6/17/2026 6:17:10 AM.
This article is licensed under a Creative Commons Attribution 3.0 Unported Licence.

Table 1 Summary of synthetic methods conducted in two steps: hotplate heating (brown labels, **H1–H4**), microwave (blue, **MW1–MW5**) and sonication (green, **S1**). Chemical formulae and single crystal XRD structures of the synthesised complexes **1–4** are shown. **2′** is a monoclinic polymorph of **2**. Ac = acetone

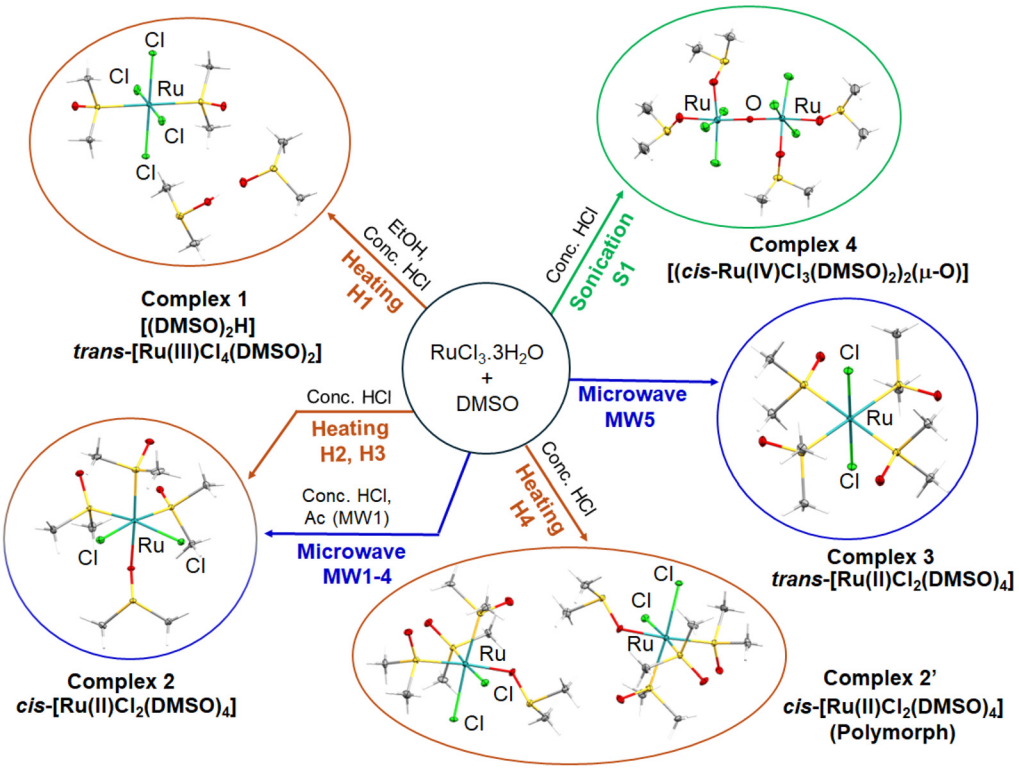

Reaction	Temp. 1 (K)	Time (min)	Temp. 2 (K)	Time (min)	Reaction	Temp. 1 (K)	Time (min)	Temp. 2 (K)	Time (min)
H1	368	180	353	15	**MW1**[a]	353	5	373	15
H2	353	20	373	60	**MW2**	353	5	373	15
H3	353	20	373	30	**MW3**	353	5	373	10
H4	353	20	373	90	**MW4**	353	5	373	20
S1	313[c]	40	—	—	**MW5**[b]	353	5	373	15

[a] Acetone was added in the beginning [b] No conc. HCl was added. [c] Max. temperature reached after 40 min sonification. Full description of protocols are found at the SI.

Fig. S2–S4). Di-Ru(IV) complex is diamagnetic with sharp ^{1}H-NMR peaks (Fig. S2). Other reported oxo-bridged Ru(IV) complexes also showed diamagnetic NMR behaviour, and this can be associated with the antiferromagnetic coupling of the metal centres resulting in diamagnetism or partial paramagnetism,[44–46] where the Ru–O–Ru angle close to 180° favours the coupling of the two metal centres.[47] Furthermore, it was reported that the strength of antiferromagnetic coupling increases with decreasing Ru–O(oxo) bond distance, within the range of 1.7774(1)–1.816(1) Å.[44] This trend is consistent with the Ru–O(oxo) bond length observed here, which is short at 1.7673(5) Å and a Ru–O–Ru angle of 178.4(4)°. Complex **4** appears to be the first reported oxo-bridged Ru(IV) dimer synthesised using sonication methods from a mononuclear Ru starting material.

In all the procedures used here (**H1–H4**, **MW1–MW5** and **S1**), single crystals suitable for XRD studies were obtained. SCXRD experiments confirmed the identity of the synthesised compounds (Fig. S4), while PXRD (Fig. S3) confirmed that the bulk material corresponds to the same phase as analysed by SCXRD. The crystallographic data, including a list of selected bond lengths and angles for all the complexes, are summarised in Tables S2–S5.

The crystal structure of complex **1**, $[(DMSO)_2H]$*trans*-$[RuCl_4(DMSO)_2]$, solved at 250 K (this work, Table S2 and Fig. S4A) and at 298 K (reported) has a monoclinic space group $P2/n$.[48] However, at a lower temperature of 100 K, an unreported phase transition from $P2/n$ monoclinic to $P\bar{1}$ triclinic (Tables S2 and S4 and Fig. S4B) was observed. Differential scanning calorimetry (DSC) of complex **1** confirmed this transition, giving an endothermic event in the range of 163–133 K (Fig. S5A). Attempts to determine the crystal structure within this temperature range were unsuccessful, as the crystals fractured, resulting in poor data quality. Reliable diffraction data of **1** at 100 K were eventually obtained after several attempts by gradually lowering the temperature. The resulting triclinic $P\bar{1}$

Open Access Article. Published on 19 December 2025. Downloaded on 6/17/2026 6:17:10 AM. This article is licensed under a Creative Commons Attribution 3.0 Unported Licence.

structure (100 K) differs from the monoclinic $P2/n$ form (298 K) primarily by the supramolecular arrangement (Fig. S5B and S5C). A crystal packing view along the *a*-axis at 298 K shows that the molecules are parallel to each other with respect to the Cl–Ru–Cl vector, while at 100 K, molecules are twisted by approximately 11°, as illustrated in Fig. S5D.

The crystals of *cis*-$[RuCl_2(DMSO)_4]$ (**2**) obtained from methods **H2–H3**, and **MW1–MW4** had an orthorhombic *Pccn* space group (Table S2 and Fig. S4C) with similar bond distances as those reported.[49,50] A search in the Cambridge Structural Database (version CSD 6.00 updated in April 2025) revealed twelve crystal structures deposited for **2**, including five distinct polymorphs.[51] These polymorphs display different three-dimensional arrangements and intermolecular interactions that stabilise the crystal packing, as summarised in Table S6. During hotplate preparation **H4**, complex **2′** crystallised in the chiral space group $P2_1$ (Tables S2 and S4 and Fig. S4D), characterised by the presence of two molecules in the asymmetric unit which differ in their molecular configuration of all S-bonded DMSO ligands, Fig. S6. Although achiral species similar to **2′** generally show a strong preference for centrosymmetric space groups, crystallisation in a Sohncke group such as $P2_1$ has previously been reported in which a small fraction of achiral molecules adopted chiral space groups, due to packing interactions favouring a chiral arrangement in the solid state.[52] Thus, complex **2′** represents one of these less common but well-established cases, which may be facilitated by the ability of the DMSO ligands to adopt different orientations through rotation about the Ru–S or Ru–O axes, reducing the overall molecular symmetry and enabling a chiral packing.

The *trans*-$[RuCl_2(DMSO)_4]$ complex (**3**) obtained from microwave method **MW5**, crystallised in the tetragonal system with an $I4/m$ space group (Table S2 and Fig. S4E). The Ru–Cl and Ru–S bond lengths, as well as the Cl–Ru–Cl, Cl–Ru–S and S–Ru–S bond angles, are in good agreement with literature values.[48]

The new compound **4**, obtained by sonication-assisted method **S1**, crystallised in the orthorhombic space group *Ibca*, Table S2. Each of the two Ru(IV) centres is structurally identical with the oxo bridge ligand located on an inversion centre and chloride ligands in a *mer*-configuration. Interestingly, in **4**, the DMSO ligands are exclusively O-bound, while complexes **1** and **3** have S-bound DMSO ligands, whereas **2** has one O-bound and three S-bound DMSO ligands. This can be related to the hardness of Ru(IV) compared to Ru(II) and Ru(III), with consequent DMSO coordination through O in **4**. The Ru–O–(DMSO) distances for **4** are 2.043(4) and 2.055(4) Å. This appears to be the first reported X-ray crystal structure of [Ru(IV)(DMSO–O)]. The Ru–O (oxo) bond length is 1.7673(5) Å with a slight deviation of Ru–O–Ru bond angle from linearity (at 178.4(4))°, comparable with other reported oxo-bridged dinuclear Ru(IV) complexes.[44] High oxidation state ruthenium dimers with an oxo bridge such as Ru(IV)–O–Ru(IV) and Ru(III)–O–Ru(III) are well represented in the literature, especially those with polypyridyl and aqua ligands. For instance, in a Ru(IV)–O–Ru(IV) dimer,[47] the Ru–O and Ru–OH_2 bond lengths were similar (~1.85 Å), whereas a Ru(III)–O–Ru(III) complex[53] displayed Ru–O and Ru–OH_2 distances of 1.87 Å and 2.14 Å, respectively, which are comparable to the values observed for **4**. Notably, the substantially shorter Ru–O distance observed in **4** suggests the formation of a bond with pronounced multiple bond character within the Ru–O–Ru moiety.[54] This structural feature is likely to induce elongation of the Ru–O–DMSO and Ru–Cl bonds as a consequence. Complex **4** exhibits a twisted geometry, with a dihedral angle of *ca.* 29° between the planes defined by O1, Cl2, Cl3, and O3 at each Ru centre of **4**, Fig. 2A. The Ru–Ru distance is 3.5344(6) Å. DFT optimisation of **4** converged to a geometry consistent with the X-ray structure, Fig. S7A.

UV-vis spectra of complexes **1–4** in acetonitrile were recorded (Fig. S8). Spectra of complexes **1–3** are in agreement with previously reported data,[36,55] while complex **4** showed a broad absorption with a maximum at 463 nm (ε = 9900 L mol^{-1} cm^{-1}). TD-DFT calculations (Table S7) are in good agreement with the experimental observations and assign the observed absorption band to ligand field and LMCT (Cl_p,d_{xy} → LUMO (d_{x^2}–d_{y^2} + O_{px})) transitions.

The electrochemical properties of **1–4** were investigated by cyclic voltammetry (CV) in acetonitrile under N_2 at 295 K from 2.0 V to −2.0 V, Fig. S9 and Table S8. For **1–4**, numerous quasi-reversible and irreversible peaks for cathodic and anodic waves were seen for all complexes.[56–58] The assignment of observed peaks to a particular oxidation/reduction process is difficult due to rapid ligand labilisation of Cl^- and DMSO and S/O isomerisation, giving new electrochemically-active species.[57,59]

Hydrolysis of **4** studied by UV-vis spectroscopy showed that within an hour **4** hydrolysed. The peak at 455 nm decreased in intensity and a new peak at 409 nm emerged in the first 10 min and then decreased over time, Fig. 2B–D. Moreover, a clear isosbestic point is present at 495 nm, suggesting conversion of **4** into a hydrolysis product. This process was also studied by ^{1}H-NMR (**4**, 10 mM). The peaks assigned to DMSO ligands disappeared with concomitant formation of four new peaks at 3.26, 2.81, 2.46 and 1.98 ppm, Fig. S10, assignable to hydrolysis products.

The reaction between complex **4** and 0.5, 1 and 2 mol equiv. of the reducing agent ferrocene (Fc) in acetonitrile was studied using UV-vis spectroscopy (**4**, 0.1 mM) and monitored every minute for 30 min, Fig. 2E, F and S11. The electron transfer between Fc and **4** was complete in *ca.* 30 min with yellow solution changing to green. In the UV-vis spectra, the peak at 466 nm decreased steadily while new peaks at 360 nm and 620 nm emerged. Moreover, initial isosbestic points at 423 nm and 492 nm shifted over time to 391 nm and 508 nm, suggesting a complicated reaction with several steps.

The peak at 620 nm contains an overlap of absorptions for ferrocenium (Fc^+) and reduced **4** (Fig. S12), and thus the absorption at 660 nm was used to monitor the progress of the reaction. This region has no absorption due to Fc^+ and the observed absorption is due to the formation of reduced **4** (**4-red**). In the first 20 min, the reaction between 0.5, 1 and 2

 This journal is © The Royal Society of Chemistry 2026

Open Access Article. Published on 19 December 2025. Downloaded on 6/17/2026 6:17:10 AM.
This article is licensed under a Creative Commons Attribution 3.0 Unported Licence.

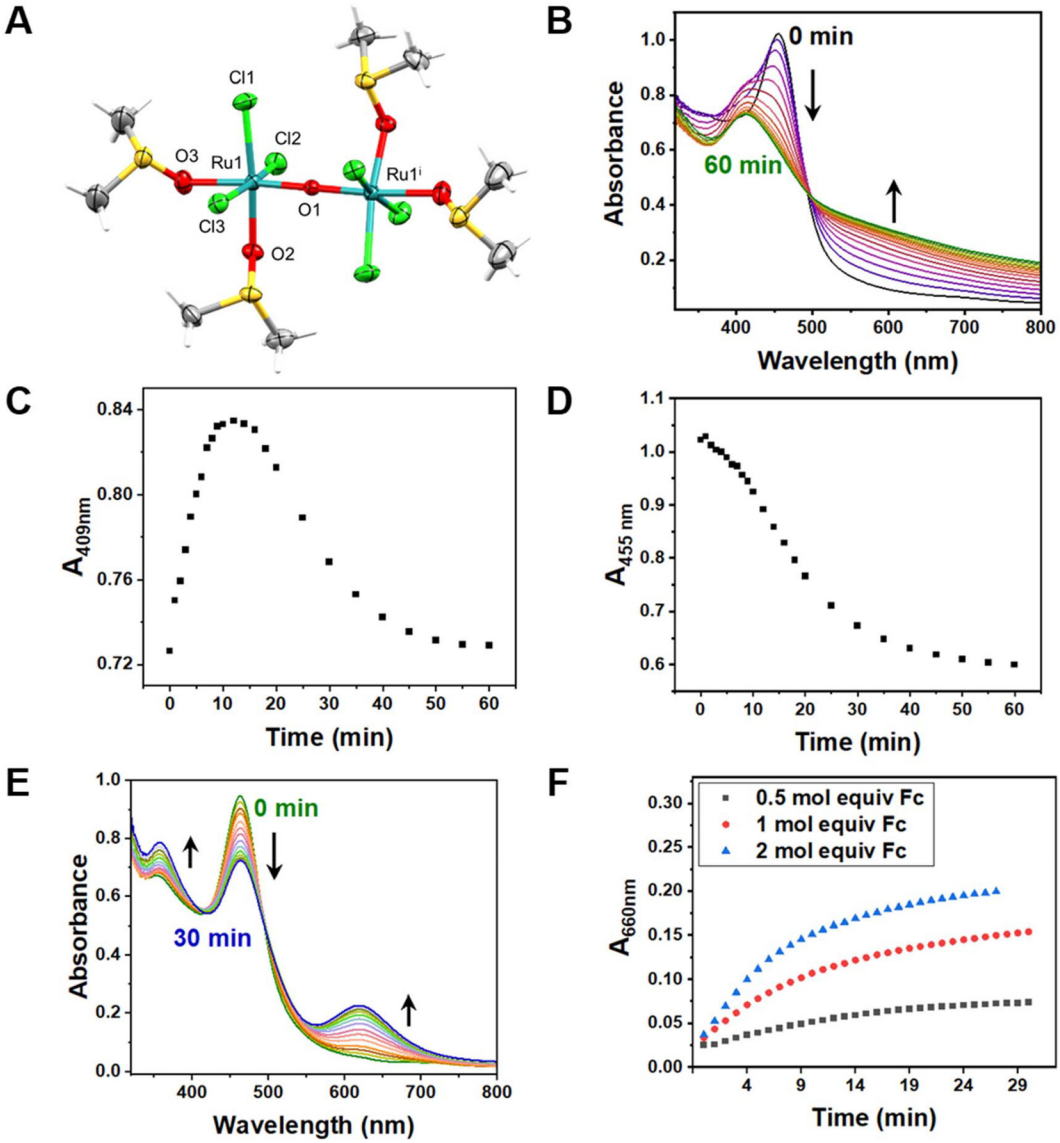

Fig. 2 (A) X-ray crystal structure of complex **4** with thermal ellipsoids displayed at 50% probability. The disorder of DMSO molecules *trans* to the oxo ligand (with positional occupancy of 0.5) has been omitted for clarity (B) UV-vis spectra for hydrolysis of complex **4** (0.1 mM in water, 1 h). (C) Time dependence of absorbance at 409 nm and (D) 455 nm for hydrolysis of complex **4**. (E) UV-vis spectra for the reaction of complex **4** with 1 mol equiv. ferrocene in acetonitrile, monitored for 30 min. (F) Change in absorbance at 660 nm *vs.* time for reactions between complex **4** and 0.5, 1 and 2 mol equiv. of ferrocene in acetonitrile.

equiv. of Fc and **4** followed pseudo-first kinetics with k_{obs} = 0.099 ± 0.003 min^{-1}, 0.099 ± 0.001 min^{-1} and 0.126 ± 0.001 min^{-1}, respectively (Fig. S13). This may indicate an initial rate-determining slow step involving a ligand substitution or electron transfer within the complex that does not depend on the Fc concentration.

When this reaction was monitored in CD_3CN by ^{1}H-NMR spectroscopy (**4**, 10 mM) in the presence of 2 mol equiv. of Fc, the peaks at 2.51 ppm and 3.00 ppm disappeared with concomitant broadening of the solvent peaks, $(CD_2H)CN$ and a trace of H_2O (Fig. S14). From HRMS, two major species were detected in solution; the observed m/z = 569.851 peak corresponds to $[Ru_2(\mu\text{-}O)(DMSO)_2Cl_2(MeCN)_3 + H]^+$ (calc. m/z = 569.856) and the m/z = 546.8229 peak can be assigned to $[Ru_2(\mu\text{-}O)Cl_4(MeCN)_4 + Na]^+$ (calc. m/z = 546.773) (Fig. S15). Their isotopic distributions confirm the presence of binuclear ruthenium species in solution. Therefore, the oxo bridge appears to be retained after initial interaction with Fc, at least partially.

An estimation of the reaction energy for conversion of **4** (Ru(IV/IV)) into its one-electron reduced form **4-red** (Ru(III/IV)) by DFT calculations revealed the highly endothermic character of the process, *ca.* −400 kJ mol^{-1} (Fig. S7B, 16 and Table S7). TD-DFT calculations for **4-red** gave a band at *ca.* 790 nm (NIR)

Open Access Article. Published on 19 December 2025. Downloaded on 6/17/2026 6:17:10 AM. This article is licensed under a Creative Commons Attribution 3.0 Unported Licence.

due to a d–d transition with a low extinction coefficient, (Table S7). The wavelength of the simulated **4-red** peak differs from that observed (620 nm) by 170 nm, suggesting the presence of different species in solution. Another model was studied involving full replacement of DMSO ligands by acetonitrile to give **4a**, *cis*-[(Ru(IV)Cl_3(MeCN)$_2$)$_2$(μ-O)]. The UV-vis transitions for both **4a** and **4a-red** (Ru(III/IV)) were calculated (Table S7). However, the spectrum of **4a-red** showed a weak peak at *ca.* 1104 nm with a low extinction coefficient, which differed considerably from experimental observations. Thus, it appears that replacement of DMSO by MeCN, followed by reduction by Fc does not describe the course of the observed reaction. Further studies would be needed to investigate the details of the mechanism.

Taking both experimental and theoretical studies into account, the solution behaviour of **4** is notably atypical. Hydrolysis studies indicate that the initial step involves displacement of the Cl^- and DMSO ligands with aqua ligands, as confirmed by the appearance of new peaks (Fig. 2B and S10). Electron transfer between **4** and Fc is complicated and not a simple 1-electron transfer. UV-vis spectroscopy revealed multiple isosbestic points during the reaction, a complexity supported by DFT calculations (Fig. 2B, S11, S14 and S16). Further insight into the reaction mechanism between **4** and Fc was provided by HRMS (Fig. S15). Analysis of isotopic distributions and mass spectral peaks suggests that the oxo-bridge remains intact, with DMSO ligands preferentially displaced by solvent molecules, while the Cl^- ligands largely remain coordinated to the metal centre, thereby stabilising complex **4**. However, it remains unclear whether ligand displacement or metal reduction occurs as the primary step in this process.

In summary, ruthenium–DMSO complexes **1–4** were synthesised by microwave and sonication assistance and compared to conventional hotplate methods. Use of microwaves led to similar products as hotplate syntheses, however with significantly reduced reaction times and improved yields for **2** and **3**. Complex **4** is a new bimetallic oxo-bridged Ru(IV) species synthesised using sonication. This study contributes to the optimisation of the synthesis of commonly used intermediates related to drugs of medicinal interest and illustrates the complexity of Ru–DMSO chemistry involving three oxidation states, both S- and O-bound DMSO ligands and a variety of isomers.

Conflicts of interest

There are no conflicts to declare.

Data availability

The data supporting this article have been included as part of the supplementary information (SI). Supplementary information is available. See DOI: https://doi.org/10.1039/d5dt02617b.

CCDC 2483730 (**1** at 100 K), 2483731 (**1** at 250 K), 2483732 (**2**), 2483733 (**2′**), 2483734 (**3**), 2483735 (**4**) contain the supplementary crystallographic data for this paper.[60a–f]

Acknowledgements

The authors would like to thank Warwick Chancellor's International Scholarship (S. N.), EPSRC (grant no. EP/F034210/1 and EP/V007688/1 (P. J. S.)) for their support for this work, and Warwick Technical Services and RTPs for their excellent assistance. RSC thanks CNPq for financial support (grant: 201190/2024-9; 315204/2023-0) and FAPEMIG (grant: APQ-01963-23). EEG thanks Warwick Institute of Advanced Studies (IAS) for his fellowship. VS and JAW are grateful to NANOKAT Initiative for financial support and Allianz für Hochleistungsrechnen Rheinland–Pfalz (AHRP) for providing CPU-time within the project RPTU-SPINPLUSXA4. We thank Prof. Richard I. Walton for use of the microwave reactor (Monowave 200 microwave).

References

1 I. Bratsos and E. Alessio, *Eur. J. Inorg. Chem.*, 2018, **26**, 2996.
2 E. Alessio, *Chem. Rev.*, 2004, **104**, 4203.
3 S. A. Elsayed, S. Harrypersad, H. A. Sahyon, M. A. El-Magd and C. J. Walsby, *Molecules*, 2020, **25**, 4284.
4 M. Oszajca, M. Flejszar, A. Szura, P. Dróżdż, M. Brindell and K. Kurpiewska, *Front. Chem.*, 2024, **12**, 2296.
5 D. P. Dorairaj, Y.-F. Lin, J. Haribabu, T. Murugan, M. Narwane, R. Karvembu, M. A. Neelakantan, C.-L. Kao, C.-C. Chiu and S. C. N. Hsu, *J. Inorg. Biochem.*, 2021, **223**, 111545.
6 E. Alessio, *Eur. J. Inorg. Chem.*, 2017, **12**, 1549.
7 S. J. Dougan and P. J. Sadler, *Chimia*, 2007, **61**, 704.
8 C. Monti-Bragadin, M. Giacca, L. Dolzani and M. Tamaro, *Inorg. Chim. Acta*, 1987, **137**, 31.
9 M. Coluccia, G. Sava, F. Loseto, A. Nassi, A. Boccarelli, D. Giordano, E. Alessio and G. Mestroni, *Eur. J. Cancer*, 1993, **29**, 1873.
10 M. Brindell, E. Kuliś, S. K. C. Elmroth, K. Urbańska and G. Stochel, *J. Med. Chem.*, 2005, **48**, 7298.
11 S. Cauci, E. Alessio, G. Mestroni and F. Quadrifoglio, *Inorg. Chim. Acta*, 1987, **137**, 19.
12 J. M. Davey, K. L. Moerman, S. F. Ralph, R. Kanitz and M. M. Sheil, *Inorg. Chim. Acta*, 1998, **281**, 10.
13 S. Cauci, P. Viglino, G. Esposito and F. Quadrifoglio, *J. Inorg. Biochem.*, 1991, **43**, 739.
14 X. Wang, B. Zhang, C. Zhao, Y. Wang, L. He, M. Cui, X. Zhu and W. Du, *J. Inorg. Biochem.*, 2013, **128**, 1.
15 K. Cao, Y. Zhu, Z. Hou, M. Liu, Y. Yang, H. Hu, Y. Dai, Y. Wang, S. Yuan, G. Huang, J. Mei, P. J. Sadler and Y. Liu, *Angew. Chem., Int. Ed.*, 2023, **62**, e202215360.
16 I. Bratsos and E. Alessio, in *Inorganic Syntheses*, ed. T. B. Rauchfuss, John Wiley & Sons, 2010, ch. 8, p. 148.

This journal is © The Royal Society of Chemistry 2026

Open Access Article. Published on 19 December 2025. Downloaded on 6/17/2026 6:17:10 AM. This article is licensed under a Creative Commons Attribution 3.0 Unported Licence.

17 G. S. P. Garusinghe, S. M. Bessey, C. Boyd, M. Aghamoosa, B. G. Frederick, M. R. M. Bruce and A. E. Bruce, *RSC Adv.*, 2015, **5**, 40603.
18 A. Vidal, R. Calligaro, G. Gasser, R. Alberto, G. Balducci and E. Alessio, *Inorg. Chem.*, 2021, **60**, 7180.
19 E. Gabano and M. Ravera, *Molecules*, 2022, **27**, 4249.
20 D. F. da Silva, J. P. A. Bomfim, R. C. Marchi, J. C. Amaral, L. S. Pinto, R. M. Carlos, A. G. Ferreira, M. R. Forim, J. B. Fernandes, M. F. G. F. da Silva, R. C. de Oliveira, D. Buss, W. D. J. Kirk and T. J. A. Bruce, *J. Braz. Chem. Soc.*, 2022, **33**, 772.
21 S. Zhang, Q. Wu, H. Zhang, Q. Wang, X. Wang, W. Mei, X. Wu and W. Zheng, *J. Inorg. Biochem.*, 2017, **176**, 113.
22 J. Jancik, A. J. Prochazkova, M. C. Scharber, A. Kovalenko, J. Másilko, N. S. Sariciftci, M. Weiter and J. Krajcovic, *Cryst. Growth Des.*, 2020, **20**, 1388.
23 G. Yang, Y. Kong, W. Hou and Q. Yan, *J. Phys. Chem. B*, 2005, **109**, 1371.
24 S. H. Jhung, T. Jin, Y. K. Hwang and J.-S. Chang, *Chem. – Eur. J.*, 2007, **13**, 4410.
25 C. O. Kappe, *Angew. Chem., Int. Ed.*, 2004, **43**, 6250.
26 A. Malhotra, W. Chen, H. Goyal, P. J. Plaza-Gonzalez, I. Julian, J. M. Catala-Civera and D. G. Vlachos, *Ind. Eng. Chem. Res.*, 2021, **60**, 6835–6847.
27 S. Wu, Y. Song, X. Wang, J. Xu, B. Xiao and K. Qiao, *Chem. Eng. Sci.*, 2022, **250**, 117386.
28 J. Rae, M. Ashokkumar, O. Eulaerts, C. von Sonntag, J. Reisse and F. Grieser, *Ultrason. Sonochem.*, 2005, **12**, 325–329.
29 K. Muthoosamy and S. Manickam, *Ultrason. Sonochem.*, 2017, **39**, 478.
30 J. H. Bang and K. S. Suslick, *Adv. Mater.*, 2010, **22**, 1039.
31 A. Ranjan, S. Singh, R. S. Malani and V. S. Moholkar, *RSC Adv.*, 2016, **6**, 65541.
32 T. Sanjurani, S. Paul and P. Barman, *Bioorg. Chem.*, 2024, **146**, 107281.
33 S. H. Crosby, G. J. Clarkson, R. J. Deeth and J. P. Rourke, *Organometallics*, 2010, **29**, 1966–1976.
34 T. Diao, P. White, I. Guzei and S. S. Stahl, *Inorg. Chem.*, 2012, **51**, 11898–11909.
35 Md. A. Arafath, F. Adam, M. B. K. Ahamed, M. R. Karim, Md. N. Uddin, B. M. Yamin and A. Abdou, *J. Mol. Struct.*, 2023, **1278**, 134887.
36 E. Alessio, G. Balducci, M. Calligaris, G. Costa, W. M. Attia and G. Mestroni, *Inorg. Chem.*, 1991, **30**, 609.
37 D. Benitez and W. A. Goddard, *J. Am. Chem. Soc.*, 2005, **127**, 12218.
38 S. Cheng, W. Wei, X. Zhang, H. Yu, M. Huang and M. Kazemnejadi, *Green Chem.*, 2020, **22**, 2069.
39 J. Mola, I. Romero, M. Rodríguez, F. Bozoglian, A. Poater, M. Solà, T. Parella, J. Benet-Buchholz, X. Fontrodona and A. Llobet, *Inorg. Chem.*, 2007, **46**, 10707.
40 C. Sens, M. Rodríguez, I. Romero, A. Llobet, T. Parella, B. P. Sullivan and J. Benet-Buchholz, *Inorg. Chem.*, 2003, **42**, 2040.
41 A. R. Costa, T. I. de Menezes, R. R. Nascimento, P. N. M. dos Anjos, R. B. Viana, A. G. A. Fernandes and R. L. S. R. Santos, *J. Therm. Anal. Calorim.*, 2019, **138**, 1683.
42 A. Chandra, P. Basu, S. Raha, P. Dhibar and S. Bhattacharya, *Dalton Trans.*, 2024, **53**, 10675.
43 T. B. Silva, D. M. Martins, P. D. S. Gois, P. Borim, P. I. S. Maia, V. P. Carvalho and B. S. Lima-Neto, *Inorg. Chem. Commun.*, 2020, **112**, 107749.
44 M. Orts-Arroyo, I. Castro, F. Lloret and J. Martínez-Lillo, *Cryst. Growth Des.*, 2020, **20**, 2044.
45 T. Misawa-Suzuki and H. Nagao, *Dalton Trans.*, 2023, **52**, 2863.
46 T. Misawa-Suzuki, Y. Kataoka, S. Mafune, T. Niwa and H. Nagao, *Dalton Trans.*, 2025, **54**, 2937.
47 I. López, S. Maji, J. Benet-Buchholz and A. Llobet, *Inorg. Chem.*, 2015, **54**, 658–666.
48 J. S. Jaswal, S. J. Rettig and B. R. James, *Can. J. Chem.*, 1990, **68**, 1808.
49 E. Alessio, G. Mestroni, G. Nardin, W. M. Attia, M. Calligaris, G. Sava and S. Zorzet, *Inorg. Chem.*, 1988, **27**, 4099.
50 A. Mercer and J. Trotter, *J. Chem. Soc., Dalton Trans.*, 1975, **23**, 2480.
51 J. Bernstein, *Polymorphism in Molecular Crystals*, Oxford University Press, Oxford, 2020.
52 E. Pidcock, *Chem. Commun.*, 2005, **27**, 3457–3459.
53 J. K. Hurst, *Coord. Chem. Rev.*, 2005, **249**, 313–328.
54 Y.-R. He, M. Zhang, W.-H. Huang, X.-X. Xue, Z.-Q. Zhou, L.-N. Feng, J.-H. Yang and B. Liu, *Dalton Trans.*, 2024, **53**, 4598–4606.
55 M. Brindell, G. Stochel, V. Bertolasi, R. Boaretto and S. Sostero, *Eur. J. Inorg. Chem.*, 2007, **16**, 2353.
56 E. Reisner, V. B. Arion, M. F. C. G. da Silva, R. Lichtenecker, A. Eichinger, B. K. Keppler, V. Yu. Kukushkin and A. J. L. Pombeiro, *Inorg. Chem.*, 2004, **43**, 7083.
57 G. Costa, G. Balducci, E. Alessio, C. Tavagnacco and G. Mestroni, *J. Electroanal. Chem.*, 1990, **296**, 57.
58 M. F. C. G. da Silva, A. J. L. Pombeiro, S. Geremia, E. Zangrando, M. Calligaris, A. V. Zinchenko and V. Y. Kukushkin, *J. Chem. Soc., Dalton Trans.*, 2000, **8**, 1363.
59 E. Reisner, V. B. Arion, A. Rufińska, I. Chiorescu, W. F. Schmid and B. K. Keppler, *Dalton Trans.*, 2005, **14**, 2355.
60 (*a*) CCDC 2483730: Experimental Crystal Structure Determination, 2025, DOI: 10.5517/ccdc.csd.cc2pcjby; (*b*) CCDC 2483731: Experimental Crystal Structure Determination, 2025, DOI: 10.5517/ccdc.csd.cc2pcjcz; (*c*) CCDC 2483732: Experimental Crystal Structure Determination, 2025, DOI: 10.5517/ccdc.csd.cc2pcjd0; (*d*) CCDC 2483733: Experimental Crystal Structure Determination, 2025, DOI: 10.5517/ccdc.csd.cc2pcjf1; (*e*) CCDC 2483734: Experimental Crystal Structure Determination, 2025, DOI: 10.5517/ccdc.csd.cc2pcjg2; (*f*) CCDC 2483735: Experimental Crystal Structure Determination, 2025, DOI: 10.5517/ccdc.csd.cc2pcjh3.